



OPEN

Evaluation of multi-hazard map produced using MaxEnt machine learning technique

Narges Javidan¹, Ataollah Kavian¹✉, Hamid Reza Pourghasemi², Christian Conoscenti³, Zeinab Jafarian⁴ & Jesús Rodrigo-Comino^{5,6}✉

Natural hazards are diverse and uneven in time and space, therefore, understanding its complexity is key to save human lives and conserve natural ecosystems. Reducing the outputs obtained after each modelling analysis is key to present the results for stakeholders, land managers and policymakers. So, the main goal of this survey was to present a method to synthesize three natural hazards in one multi-hazard map and its evaluation for hazard management and land use planning. To test this methodology, we took as study area the Gorganrood Watershed, located in the Golestan Province (Iran). First, an inventory map of three different types of hazards including flood, landslides, and gullies was prepared using field surveys and different official reports. To generate the susceptibility maps, a total of 17 geo-environmental factors were selected as predictors using the MaxEnt (Maximum Entropy) machine learning technique. The accuracy of the predictive models was evaluated by drawing receiver operating characteristic-ROC curves and calculating the area under the ROC curve-AUCROC. The MaxEnt model not only implemented superbly in the degree of fitting, but also obtained significant results in predictive performance. Variables importance of the three studied types of hazards showed that river density, distance from streams, and elevation were the most important factors for flood, respectively. Lithological units, elevation, and annual mean rainfall were relevant for detecting landslides. On the other hand, annual mean rainfall, elevation, and lithological units were used for gully erosion mapping in this study area. Finally, by combining the flood, landslides, and gully erosion susceptibility maps, an integrated multi-hazard map was created. The results demonstrated that 60% of the area is subjected to hazards, reaching a proportion of landslides up to 21.2% in the whole territory. We conclude that using this type of multi-hazard map may be a useful tool for local administrators to identify areas susceptible to hazards at large scales as we demonstrated in this research.

Natural disasters are serious threats to human life and properties all over the world. Preventing natural catastrophes is not conceivable, yet by developing suitable preparation plans and mitigation measures its drawbacks can be alleviated¹. Considerable morphological changes in landforms due to active tectonics or climate changes can impact control in human activities²⁻⁹. However, also humans can drastically modify natural ecosystems, negatively. For example, deforestation, non-sustainable agricultural management or human-made constructions can increase soil mobilization and the transportation of sediments, resulting in extreme land degradation processes¹⁰⁻¹³. Combining land degradation processes allow us understanding environmental issues and threats difficult to be assessed because of its complexity.

Events such as gully erosion, landslides, and floods are physical phenomena, active in geological times but uneven in time and space¹⁴⁻¹⁷. They are considered hazard events, which can be induced by humans or not, but all of them are key global issues threatening human life, resources and goods¹⁸⁻²¹. Moreover, they have different drawbacks in various places and because of their correlated subsequences, these catastrophes have contrary

¹Department of Watershed Management, Faculty of Natural Resources, Sari Agricultural Sciences and Natural Resources University (SANRU), Sari 48441-74111, Iran. ²Department of Natural Resources and Environmental Engineering, College of Agriculture, Shiraz University, Shiraz 71441- 65186, Iran. ³Department of Earth and Marine Sciences (DISTEM), University of Palermo, Palermo 90123, Italy. ⁴Department of Range Management, Sari Agricultural Sciences and Natural Resources University (SANRU), Sari 48441-74111, Iran. ⁵Department of Physical Geography, University of Trier, 54296 Trier, Germany. ⁶Soil Erosion and Degradation Research Group, Department of Geography, Valencia University, Blasco Ibàñez, 28, 46010 Valencia, Spain. ✉email: a.kavian@sanru.ac.ir; rodrigo@uni-trier.de

long-term effects. When these penalties have a considerable impact on human life and activities, they become natural disasters^{23,24}. Since human interventions in natural ecosystems that cause natural catastrophe to lead to endangering human life and significant economic consequences, the awareness of society is vital to reduce them^{25–27}. Mitigating the effects of potential catastrophes and preparing the proper infrastructure for tackling them requires notably accurate information about the vulnerability and susceptibility of a specific territory about environmental hazards²². In general, natural disasters occur more frequently overpassing the human capability to restore the effects of past events²⁸. Hence, it is necessary to plan and manage the natural catastrophes to decrease both the economic penalties and loss of humankind life. To achieve this goal, it is key to consider the natural catastrophe predictive maps throughout the land use planning stages.

Since natural hazards are difficult to be predicted, most of the studies focus on a single hazard to be mapped. However, unfortunately, it is usual that several hazards occur at the same time in one place. Therefore, there is a necessity to make integrate studies although they are more complex and difficult to be represented in one synthesized map or article. During the last years, major developments have been done to quantify the feedback, mechanisms and interconnection among different hazards and factors^{29–31}. One of the most relevant achievements are the multi-hazard mapping initiative (MMI), which started by the Federal Emergency Management Agency (FEMA) to provide multi-hazard advisory maps^{32,33} and the novel UN framework for catastrophe risk decrement sturdily highlights the necessity of a multi-hazard approach³⁴.

These models allow showing the spatial pattern of a natural phenomenon, environmental elements, or some human activities, and provide information on the spatial distribution of natural hazards such as flood, landslides, and erosion and they are important tools for planners and environmental managers to identify susceptible areas and to prioritize their mitigation response efforts^{28,35–38}. A multi-hazard susceptibility map (MHSM) represents susceptibility and hazard information, together, on a single combined map. Because of the large number of maps and their probable variance in the area covered by different scales, applying a single hazard map to supply information on every single hazard, is complicated for planners³⁹. Alternatively, a MHSM raised from the synthesis of different hazard maps would allow giving proper information from a particular area and it could help the land planners to analyze all of them from a holistic point of view. The multi-hazard map is an accurate tool to create awareness in mitigating multiple hazards⁴⁰ and also for the selection of appropriate land uses and evaluation of susceptibility areas. By the way, the United Nation has emphasized the significance of multi-hazard assessment and referred that it “is an essential element of a safer world in the twenty-first century”. Nevertheless, analyzing a multi-hazard map is complicated and requires major challenges as well as the analysis of susceptibility⁴¹.

In this regard, several types of research have focused on multi-hazard evaluation via GIS-based methods that make it possible to analyze various data and the improvement of natural hazard models for a specific area^{41–44}. For example, it is representative the research conducted by Sheikh et al. in the Golestan province at a large scale to assess a multi-hazard-based management using a coupled TOPSIS–Mahalanobis distance⁴⁵. Also, there are several inventive, statistical, and deterministic methods that can be used in a single hazard or even multi-hazards^{28,46–56}. Data-mining models have newly been suggested with predictive skills and progressive pattern learning and can present a good platform to synthesize and to analyze the information for the definition of potential hazard areas^{57–63}. The most common methods proposed in the literature are artificial neural networks^{64,65}, frequency ratio-FR^{17,66}, logistic regression⁶⁷, index-of-entropy⁶⁸, fuzzy logic⁶⁹, and multivariate adaptive regression splines^{31,70}. Also, the development of machine learning and statistical methods techniques, including support vector machine (SVM), random forest (RF), boosted regression trees (BRT), maximum entropy (MaxEnt) has contributed significantly to the field of natural hazards^{71–73}. Among these, maximum entropy has been successfully used for assessing different types of natural hazards such as landslides^{55,67}, floods⁷⁴, gully erosion⁷⁵ and soil salinity⁷⁶ due to fast and easy implementation and robust mathematical functions and theoretical backgrounds.

So, the main aims of the current research are: (1) to explore the ability of the MaxEnt model to predict the spatial occurrence of flood, landslides, and gully erosion; (2) to better understand the relationships between these processes and their controlling factors; and (3) to design a methodological perspective for preparing a combined multi-hazard map for land use planning and hazard mitigation. To achieve these goals, we present a study case in the Gorganrood Watershed, which has witnessed several landslides, gully erosion, and floods that have been a matter of debate in recent years^{77,78}.

Study area

The Gorganrood Watershed is located in the Golestan Province which is situated in the north-eastern part of Iran and covers an area of 10,197 km². The study area lies between the latitudes of 36° 34' to 38° 15' N and the longitudes of 54° 5' to 56° 8' E (Fig. 1). Topographically, it is characterized by steep slopes, up to 69° in mountainous regions. The central and western parts are generally characterized as plain and flat areas with an average elevation of between 95 and 3652 m⁷⁸. The annual mean rainfall is approximately 231–848 mm⁷⁸. The southern section has a typical mountain climate and the central and northern regions have a Mediterranean climate. The average minimum and maximum temperatures are 11 and 18.5 °C, respectively⁸⁰. In the last decade, this area has been challenged with different natural hazards such as erosion, landslides, and floods which was selected as an appropriate application site for the multi-hazard probability assessment (MHPA).

According to national reports, the study area is covered with some prone lithological formations such as dark grey shale, sandstone, and Quaternary deposits⁷⁸. Regarding the infrastructures, the area consisted of main cities, villages, and 1218 km of national roads, where to some extent, they can be exposed to a divertimento of natural hazard occurrences⁷⁸. Figure 2 presents some photographs of gully erosion locations (a, b), landslides (c, d), and flood (e) in Golestan Province.

In this area, one of the deadliest flash floods occurred on 10th August 2001 which caused up to 300 people deceased, 381 harmed, and 4000 buildings were endured heavy loss⁷⁹. Moreover, 99 mm³ (millions square meters)

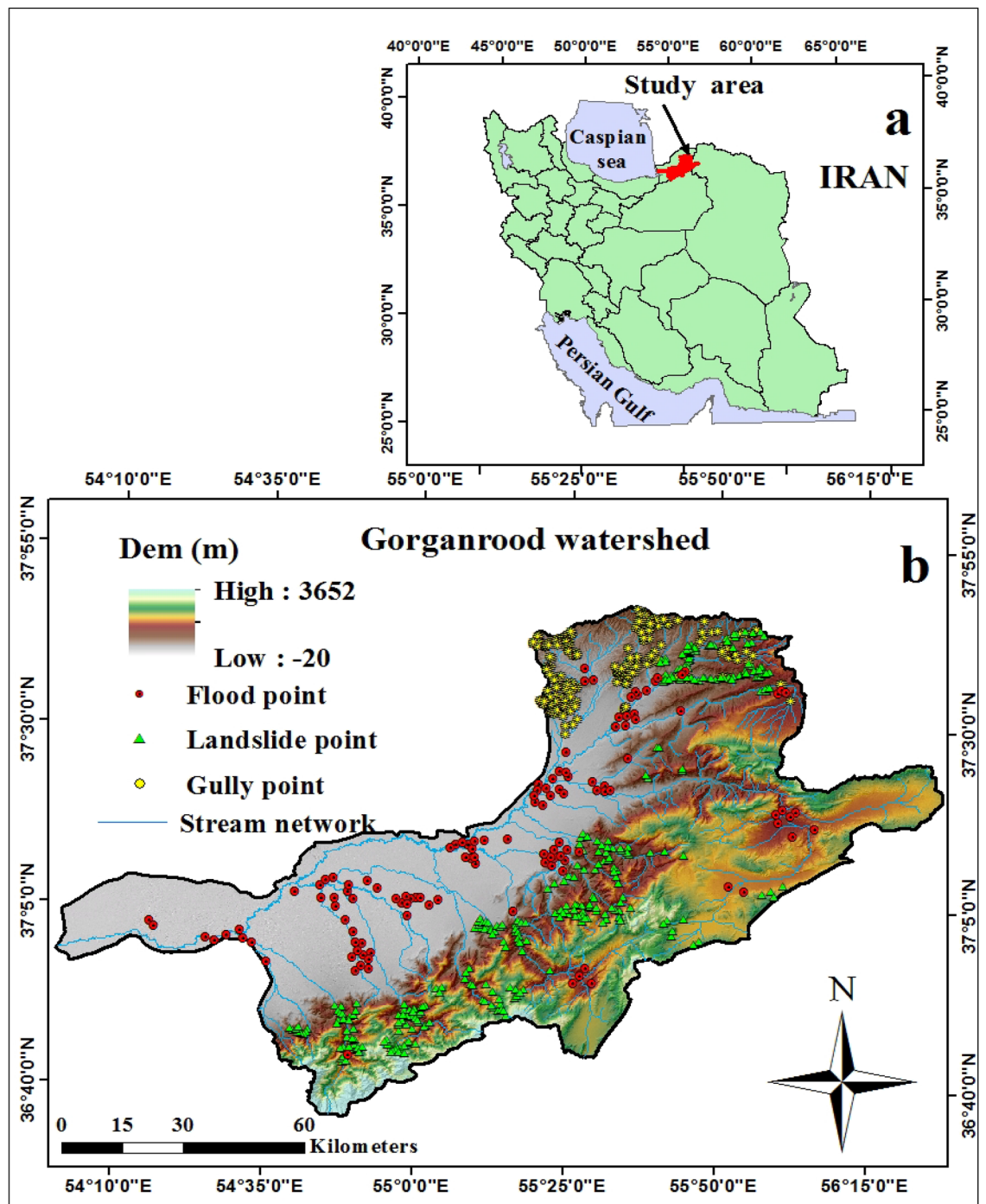


Figure 1. Location of the study area, sampling points and elevation.

of sediments loaded behind the dams, and also made damages to rangelands, forests, and residential units⁷⁸. Some authors estimated 430,000 hectares affected by erosion because of gullies, landslides, etc. from 1990 to 2005. In this province, about 5–6 t/ha/year soil erodes in forest areas⁸⁰. Also, because of the existence of the steep slopes in the study area, the landslide is one of the destructive events in the area and often destroys gardens and agricultural land, the damage of roads and natural resources⁵⁵. Loss of soil, the imposition of plenty of costs, reduced agricultural potential and has caused the migration of people in the villages of this region.

Methodology

Figure 3 illustrates the methodological flowchart of this approach that was used for the MHPM analysis using the MaxEnt model. The flowchart comprises main four steps: (1): preparing thematic layers (17 geo-environmental conditioning factor); (2): gully erosion, flood, and landslides susceptibility modelling using the ME machine learning techniques; (3): validation of the susceptibility maps using the ROC-AUC curve; and, (4) to combine

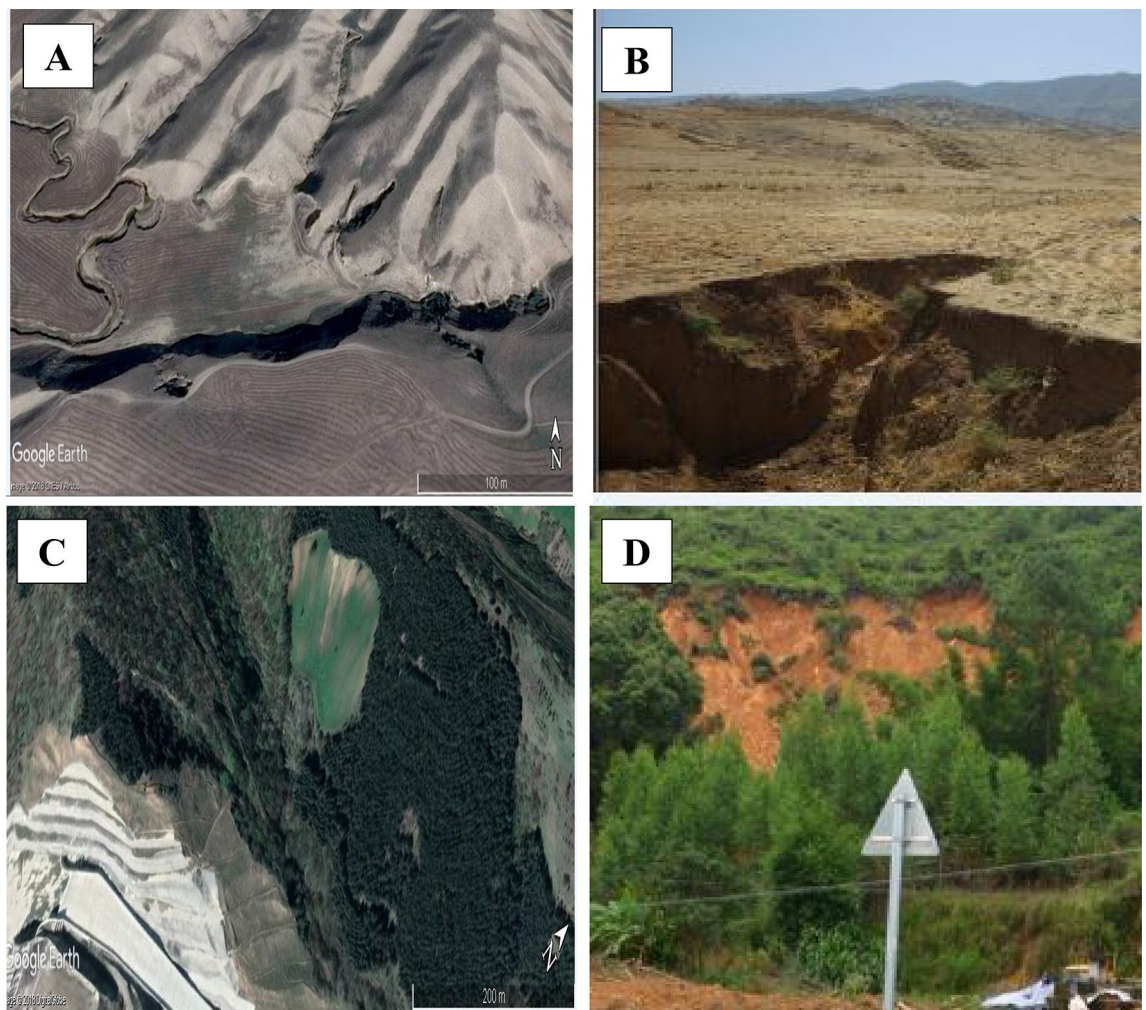


Figure 2. Some examples of gully erosion (a, b) and landslides (c, d) in the Golestan Province, Iran. *(A) and (C) were obtained from Google Earth, and (B) and (D) were taken by Narges Javidan.

flood, landslides, and gully erosion susceptibility maps to prepare a multi-hazard probability map for land use planning and hazard mitigation.

Landslides, gully erosion, and flood inventory mapping. A key step for susceptibility mapping is the preparation of an inventory of hazard landforms⁸¹. The landslide, gully erosion, and flood inventory for the Gorganrood Watershed were compiled from field investigation and national and regional documents from various organizations including the Water Resources Organization and Department of Natural Resources Management of Golestan. Considering that some hazard locations are located in mountainous areas and the field investigation may miss them, Google Earth images were used for landslides identification, as well. The inventory map for gully erosion is a collection of occurrences (283 gully locations), where a landslide inventory map is containing 351 landslide locations. Some authors highlighted that using analysis of the past documents of flood occurrences, the future flood events in an area can be estimated⁸². So, in this study, a flood inventory map was prepared by containing 127 flood locations. In general, a random partition algorithm^{83,84} was used to separate training points from the validation points. In the current study, 70% of each hazard was used in the model building (training) and the remaining 30% were used for the validation. Three replications and three sample data sets were used to perform these processes including S1, S2, and S3. These datasets were arranged to evaluate the robustness of the built models and data sensitivity^{81,85,86}. The equal data sets (positives/negatives) are applied which includes all the positive cells (hazard locations) and the same randomly inferred negative cells (non-hazard locations).

Flood, landslides, and gully erosion conditioning factors. It is essential to determine the effective factors on different natural hazards and human-made fatalities to performing flood, landslides, and gully erosion susceptibility maps, separately⁸⁷. A good understanding of the main hazards-related factors is needed to recognize the susceptible areas. For this aim, the conditioning factors for different hazards were selected from the literature review^{55,59,84,88,89}. In this study, ArcGIS 10.5 (ESRI, USA) and System for Automated Geoscientific Analyses (SAGA) software were used to produce and display these data layers. For the application of the MaxEnt machine learning model, all the factors were converted to a raster grid with 30×30 m grid cells. Entire the con-

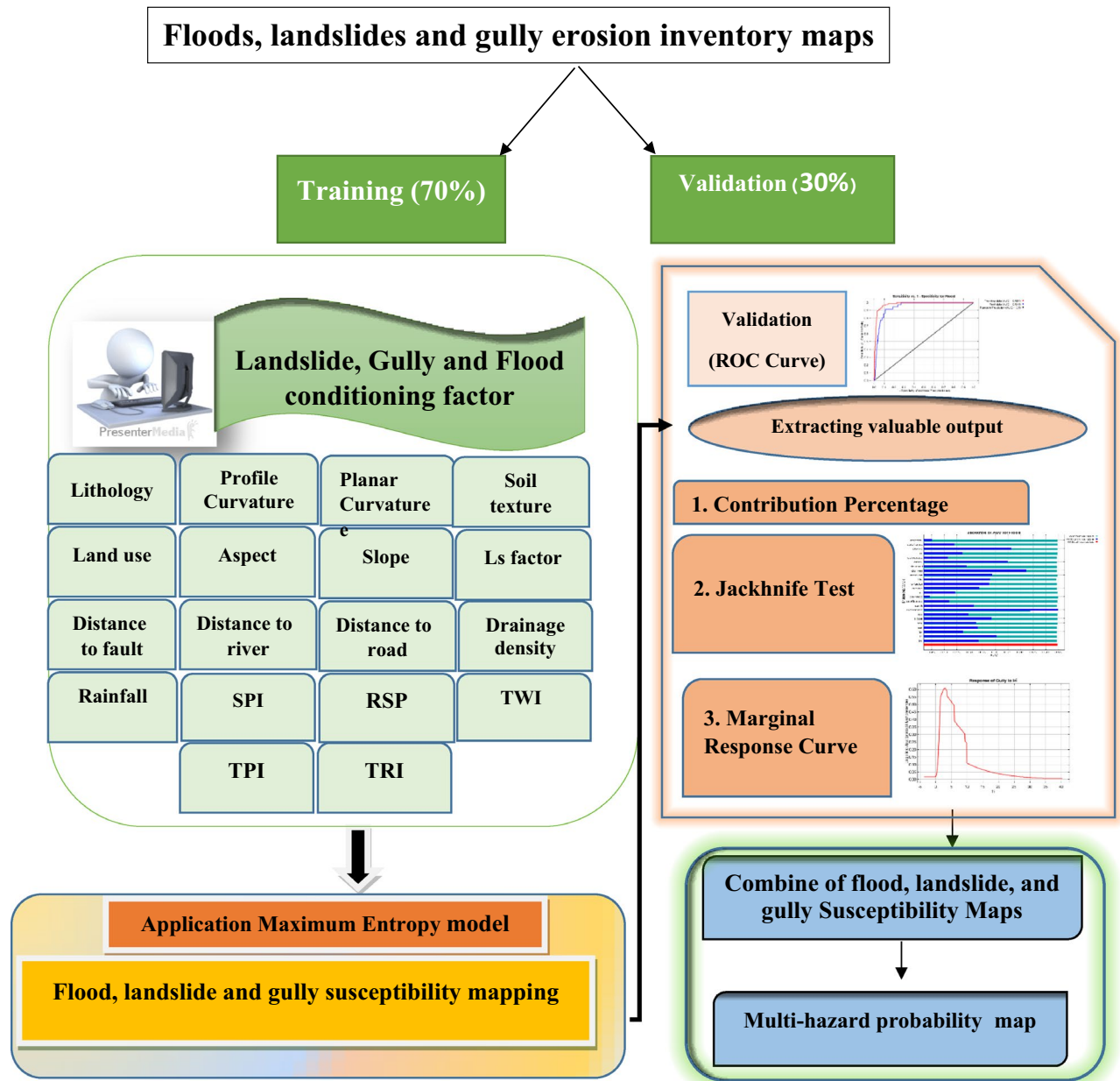


Figure 3. Flowchart of the methodology used for the MHPM in Gorganrood Watershed, Golestan Province, Iran. *Own elaboration.

ditioning factors were primarily continuous, and some of them were classified within different categories based on expert knowledge and literature review^{36,90–92}.

As in Suppl. Material 1, the predicting factors used in this study for three different types of hazards are as follows: (a) Digital Elevation Model/elevation (m), (b) slope aspect, (c) slope per cent, (d) land use, (e) plan curvature, (f) profile curvature, (g) TWI, (h) lithological units (i) drainage density (mm), (j) soil texture, (k) distance to streams (m), (l) annual mean rainfall, (m) relative slope position, and for Landslide are (n) distance to faults (m), (o) stream power index, (p) LS factor Also (q) distance to roads (m) was employed for gully erosion. Table 2 also shows the predicting factors used in this work for three hazards.

DEM (Digital Elevation Model) of the subject area with a 30 m pixel size was produced using digital contours data prepared from the Department of Natural Resources Management of Iran (Suppl. Material 1 a–c). From this DEM, some geomorphological layers such as slope^{93–96}, hillslope aspect^{97–102}, curvature layers^{103,104} were obtained using ArcGIS 10.5 software (ESRI, USA). The slope curvature map was compiled with three categories: convex, concave, and flat. Positive curvature exhibits convex ($> +0.1$), negative curvature depicts concave (< -0.1), and zero curvature represents flat (-0.1 to $+0.1$). Also, profile and plan curvatures possess a range of positive and negative values and return a different description in every single index. Positive and negative values in profile curvature demonstrate convexity (increasing flow velocity) and concavity (reducing flow velocity), respectively.

On the contrary, positive and negative values in the plan curvature denote concavity (flow convergence) and the convexity (flow divergence), respectively^{54,105}. Values close to zero represent neutral curvature in both cases.

Land use/land cover (Suppl. Material 1 d) plays a significant role in the operation of hydrological and geomorphological processes by directly or indirectly influences on evapotranspiration, infiltration, run-off generation, and sediment dynamics^{102,106}. The land use/land cover map of the subject area in 1:100,000-scale was prepared from the Natural Resources Office of Golestan Province and modified by Google Earth images. The land use/land cover of the subject area comprises of the lake, residential areas, forest lands, rangelands, drying farming, irrigation farming, rocky lands, and saline lands. Soil texture is generally recognized as a weighty controlling factor in the mechanism of infiltration and runoff generation and is effective on hazard occurrence^{107–109}.

This layer was created by digitizing the soil texture map of Golestan Province (1:100,000-scale) gained from the Agriculture Department, Iran. The soil texture in the subject area comprises of sandy-loam, clay-loam, sandy-clay-loam, silty-clay, silty-clay-loam, and silty-loam (Suppl. Material 1 g). The topographic position index (TPI) approach was applied to assess topographic slope location, and to zone ordination automation, which creates a single-band raster characterized quantities measured upon elevation¹¹⁰. It is an algorithm increasingly applied to measure topographic slope positions and displays the corresponding position of each cell (Suppl. Material 1 h).

Moore and Grayson¹¹¹ and Grabs et al.¹¹² mentioned that TWI (Topographic wetness index) represents the tendency of gravitational forces and the spatial distribution of wetness conditions to move water to the downslope. This factor has been prepared using Eq. (2):

$$TWI = \ln\left(\frac{\alpha}{\tan\beta}\right) \quad (1)$$

where α is the cumulative upslope area draining through a point (per unit contour length) and $\tan\beta$ is the slope angle at the point. In this survey, the TWI map was prepared in SAGA-GIS and its value ranges from 1.20 to 22.92 (Suppl. Material 1 i).

Distance to streams is one of the key conditioning factors due to its importance on the flood magnitude and spread of landslides and gully erosion^{48,113}. Layers of the proximity were produced using the Euclidean distance function in ArcGIS 10.5 software and varying from 0 to 11,720 m for roads (Suppl. Material 1 r), 0–15,080 m for streams (Suppl. Material 1 j), and 0–55,212 m for faults (Suppl. Material 1 s). The roads and rivers were derived from the national topographic map at the scale of 1:50,000 whereas faults extracted from geology map in 1:100,000-scale. Based on field studies, landslides are distributed typically nearby the linear features especially faults and roads. Landslide hazard level is closely related to the proximity to faults and roads. It affects not only surface structures but also terrain permeability^{100,101,114}. Where water flow concentrates may be appropriate for hosting gullies, road construction undoubtedly has a sturdy negative impact on slope stability¹¹⁵. The drainage density (Suppl. Material 1 k) is also one of the main conditioning factors that strongly contribute to many hazards' occurrence⁵⁹. According to Tehrani et al.⁸⁸, a high drainage density causes a larger surface runoff ratio. The drainage pattern of a region is influenced by different factors such as the structure and nature of the soil characteristics, geological formation, infiltration rate, slope degree, and vegetation cover condition⁸³. To convert the drainage network pattern to measurable quantity, the drainage density was determined using an extension of "line density" in ArcGIS 10.5 software. Rainfall-triggered landslides have brought great damages to communication sub-structures, properties, and pasture biomass production^{116–118}. The annual mean rainfall map of Gorganrood Watershed was prepared based on the rainfall data extracted from the Regional Water Organization of Golestan Province. This map created using fifty-three stations and a statistical period of 2001–2016 based on the Inverse Distance Weight (IDW) interpolation method (Eq. 3). This map ranges from 384 to 810 mm/year. The rainfall map was prepared in a raster format of 30 × 30 m in ArcGIS 10.5 as an input layer for assessment of hazard (Suppl. Material 1 l).

$$\lambda_i = \frac{D_i^{-\alpha}}{\sum_{i=1}^n D_i^{-\alpha}} \quad (2)$$

where λ_i is the weight of the point i , D_i is the distance between the points i and the point of the unknown, and α is equal to the weighing power¹¹⁹. Assuming that discharge is associated with the specific catchment area, the erosive power of water flow can be measured by the stream power index-SPI (Suppl. Material 1 m)¹¹¹:

$$SPI = A_s \times \tan\sigma \quad (3)$$

where A_s represents the specific catchment area in meters and r is the slope gradient in degrees. The SPI index is one of the most important factors controlling slope erosion processes since the erosive power of running water straightly influences river cutting and slope toe erosion¹²⁰. The areas with high stream power indices have an excessive potential for erosion because it is representative of the potential energy procurable to entrain sediment¹²¹. The relative slope position (RSP), as a tool, could calculate several terrain indices from the digital elevation model (Suppl. Material 1 n). General information on the computational concept can be found in¹²². The discrepancy between the value of one cell and the average value of the 8 surrounding cells defines the TRI (Terrain Ruggedness Index)⁵¹. In the first place, the two input neighborhood raster (using a 3 × 3 neighborhood for min and max) was produced from a DEM, afterwards, the equation was run in Raster Calculator (Suppl. Material 1 o). Lithological units (Suppl. Material 1 p) play a dominant role in determining gully erosion and landslides in each area^{99,102,123,124} because gully erosion is particularly dependent on the lithology properties and various lithological units demonstrate important differences in landslide instability. Also, lithology is assumed as a necessary factor in the spatial and temporal variations of drainage basin hydrology¹²⁵. Lithological units have different susceptibility to active hydrological processes. In this study, the lithological map of the subject area

Group	Code	Formation
1	Ksr	Sarcheshmeh
2	Pz1a.bv	–
3	E1c	–
4	kl	Ruteh
5	Jch	Chamanbid
6	Pr	Ruteh limestone
7	TRJs	Shemshak
8	Cm	Mobarak
9	Cl	Lalun
10	PIQc	Kashfrud
11	Sn	Niur
12	Jmz	Mozduran
13	ksn	Sanganeh
14	Murmg	Dalichai
15	Qft	Alluvial terrace
16	Jl	Lar
17	Dp	Khoshyeylaq
18	pCmt2	Padeha
19	Ekh	Khangiran
20	Kat	Aitamir
21	Pd	Dorud
22	Jbash	Bashcalateh
23	Qsw	–
24	TRe	Elikah

Table 1. Lithology of the Gorganrood Watershed.

was produced according to the available geological maps on a scale of 1:100,000 obtained from the Geological Survey Department, Iran. Different variety of lithological formations have covered the Gorganrood Watershed which is classified into 24 groups (Table 1).

The LS (slope-length) plays as a significant factor in soil erosion and natural hazards occurrence¹²² and is known as a parameter used in the RUSLE equation to consider the effect of topography on erosion¹²⁶. The topographical factor depends on the slope steepness factor (S) and the slope length factor (L) and was estimated based on the slope and specific catchment area as follow¹²⁷:

$$LS = (As/22.13)^{0.4} \times (\sin\beta/0.0896)^{1.3} \quad (4)$$

where As is the specific catchment area and β is the slope in degrees. The LS factor map for Gorganrood Watershed (Suppl. Material 1 q) was extracted using the SAGA-GIS software¹²².

Multi-collinearity test. The factors were used to consider the effect of correlation among them as the independent variables (Table 2). When the correlation between two independent variables is considerably high, it is a problem in the modelling process. The problem is named multi-collinearity. The VIF (variance inflation factor) and tolerance are two significant indices for multicollinearity diagnosis. VIF is the reciprocal of tolerance, contrarily, tolerance is $1 - R^2$ for the regression of that variable in contradiction of all the other independents, deprived of the dependent variable¹²⁸. A VIF of > 5 or 10 and more and/or tolerance of lower than 0.10 shows a multicollinearity obstacle^{129,130}.

Maximum entropy (MaxEnt) model. The MaxEnt model was applied in the Maxent software for modelling landslides, flood, and gully erosion and calculation of hazard values (version 13.0.6.0). Phillips et al.¹³¹ proposed the MaxEnt model for predictive modeling of geographical species distribution based on the most important environmental condition when presence data are available^{131,132}. We can also explain the maximum entropy estimation from a decision-theoretic viewpoint as a sturdy Bayes estimation. MaxEnt depends on a machine learning response that makes predictions from incomplete data^{133,134}. The MaxEnt output produces in ASCII format as a continuous prediction of specific presence that ranges from 0 to 1¹³⁴. For running the MaxEnt model, validation and training datasets were processed in excel format, and the conditioning factors were converted from raster to ASCII format, which is needed in Maxent software¹³⁵. During the model running, for model training in the calibration phase, a random selection algorithm was used and (70%) of datasets were randomly selected⁸³. This machine learning technique allows for the investigation of the relationship amongst a dependent variable (landslides, flood, and gully occurrence) and several independent variables (conditioning factors/geo-environmental factors), respectively. Details are given in Phillips et al.¹³².

Flood predicting factors	Landslide predicting factors	Gully predicting factors
Elevation (m)	Elevation (m)	Elevation (m)
Slope aspect	Slope aspect	Slope aspect
Slope percent	Slope percent	Slope percent
Land use	Land use	Land use
Plan curvature	Plan curvature	Plan curvature
Profile curvature	Profile curvature	Profile curvature
Topographic wetness index	Topographic wetness index	Topographic wetness index
Lithological units	Lithological units	Lithological units
Drainage density	Drainage density	Drainage density
Soil texture	Soil texture	Soil texture
Distance to streams (m)	Distance to streams (m)	Distance to streams (m)
Annual mean rainfall (mm)	Annual mean rainfall (mm)	Annual mean rainfall (mm)
Relative slope position	Relative slope position	Relative slope position
Terrain Ruggedness Index	Terrain Ruggedness Index	Terrain Ruggedness Index
Stream power index	Stream power index	Stream power index
	Distance to faults (m)	Distance to faults (m)
–	LS factor	LS factor
–	Distance to roads (m)	Distance to roads (m)

Table 2. Predicting factors for the three selected hazards in the study area.

Considering the effect of variables importance using the MaxEnt model. In the current study, the sensitivity analyses^{136,137} has been used as an exploratory technique to define the effect of variable variations on model outputs, allowing then a quantitative evaluation of the relative importance of uncertainty sources. To assess the uncertainty of projected maps in this study, a Jackknife test was executed for investigative the effects of removing any of the conditioning factors on the three susceptibility maps¹³⁸. The Jackknife test can be used to assess the relative strengths of every predictor variable^{131,138,139}. In consonance with the Jackknife test outcomes, variables with zero values including (SPI and soil for flood modelling; SPI, LS, profile curvature, and aspect for gully erosion; and TWI for landslides) were eliminated. Therefore, the remaining variables were used to run the final model for all three hazards.

Evaluation of the predictive performance of three hazards models. The validation step is the most important process of modelling¹⁴⁰. The prediction accuracy of the built hazard models was evaluated by the ROC curve. In this approach, the AUC can evaluate the prediction accuracy qualitatively^{119,141}. The ROC curve is a methodical technique that has been using to describe the proficiency of deterministic and probabilistic and prediction systems¹⁴².

The prediction accuracy of the models based on the AUC value can be classified three classes of accuracy following the classification proposed by Hosmer & Lemeshow¹⁴³: 0.7, 0.8, and 0.9 AUC value thresholds were adopted to acceptable, excellent, and outstanding performance, respectively^{81,89}.

The multi-hazard mapping adoption process. The combination of three hazard maps was used to create the multi-hazard probability map including flood, gully erosion, and landslide. First of all, for every considered hazard in this study, the MaxEnt model was constructed. Afterwards, the multi-hazard probability map was prepared based on the three individual hazard susceptibility maps, by synthesizing the three individual susceptibility maps according to their four classes in ArcGIS 10.5 environment, and this multi-hazard susceptibility map was ultimately classified into eight classes.

Results

Results of the multi-collinearity test. According to the results of Table 3a,b,c, TRI (Terrain Ruggedness Index) for landslides, flood, and gully erosion with VIF > 5 and tolerance < 0.1 was eliminated. So, other factors are used for future analyses, and results show there is not any multi-collinearity among the remaining independent variables in the present study.

Application of the MaxEnt model. The susceptibility map for each hazard and each dataset in the study area was produced using both continuous and categorical data sets. Finally, the MaxEnt model was built using all three training groups of the sample data sets (i.e., S1, S2, S3) in the training step. Susceptibility maps of the flood, gully erosion and landslides of the study area are presented in Fig. 4. Four susceptibility groups including low (L), Moderate (M), high (H), and very high (VH) are performed based on the output susceptibility maps using the most authentic natural breaks classifying method.

Predictors	Collinearity Statistics	
	Tolerance	VIF
(a) For flood predictors		
Drainage density	0.386	2.589
Relative slope position	0.694	1.442
Slope	0.210	4.752
Soil	0.788	1.269
Stream power index	0.734	1.362
Topographic wetness index	0.656	1.525
Elevation	0.454	2.205
Distance to stream	0.428	2.335
Land use	0.902	1.109
lithology	0.687	1.455
Plan curvature	0.634	1.576
Profile curvature	0.658	1.519
Annual mean rainfall	0.547	1.828
Aspect	0.917	1.091
(b) For landslide predictors		
Plan curvature	0.729	1.372
Annual mean rainfall	0.610	1.641
Drainage density	0.334	2.997
Relative slope position	0.328	1.592
Slope percent	0.394	2.538
Soil texture	0.880	1.136
Stream power index	0.241	4.156
Elevation	0.451	2.215
Distance to fault	0.804	1.244
Distance to stream	0.311	3.217
Land use	0.857	1.167
Lithology	0.907	1.103
LS factor	0.444	2.250
Topographic wetness index	0.494	2.022
Profile curvature	0.604	1.657
Aspect	0.985	1.016
(c) For gully erosion predictors		
Plan curvature	0.639	1.564
Annual mean rainfall	0.580	1.723
Drainage density	0.385	2.598
Relative slope position	0.616	1.624
Slope percent	0.358	2.793
Soil texture	0.772	1.296
Stream power index	0.400	2.500
Topographic Wetness Index	0.557	1.796
Aspect	0.943	1.060
Elevation	0.427	2.342
Distance to road	0.733	1.364
Distance to stream	0.393	2.543
Land use	0.803	1.245
Lithology	0.818	1.222
Profile curvature	0.582	1.719

Table 3. The results of multi-collinearity test.

Also, Fig. 5 shows the relative distribution of the average of the flood, landslides, and gully erosion susceptibility classes for three categories of the sample data sets. Besides, the statistical characteristics of the probabilistic prediction of the three hazards and all sample data sets are shown in Table 4.

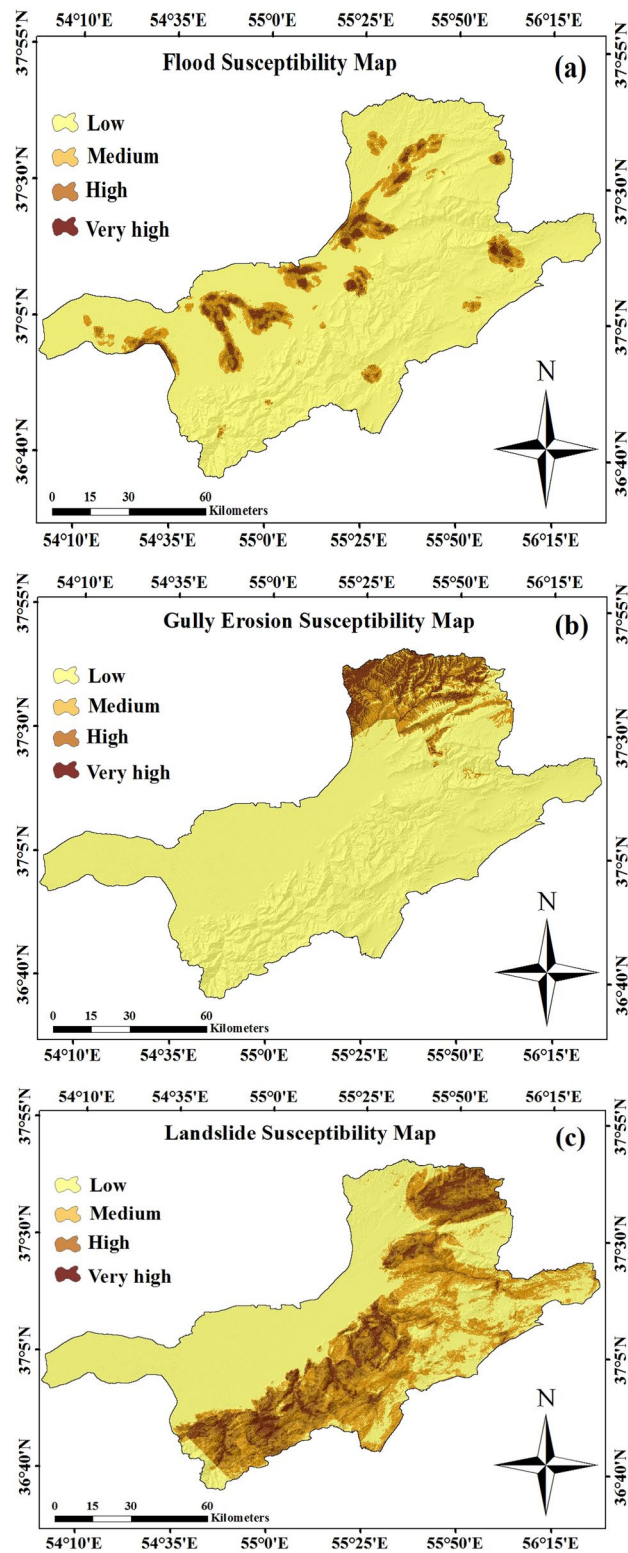


Figure 4. Susceptibility mapping for (a) floods, (b) gully erosion, (c) and landslides using MaxEnt model in the study area.

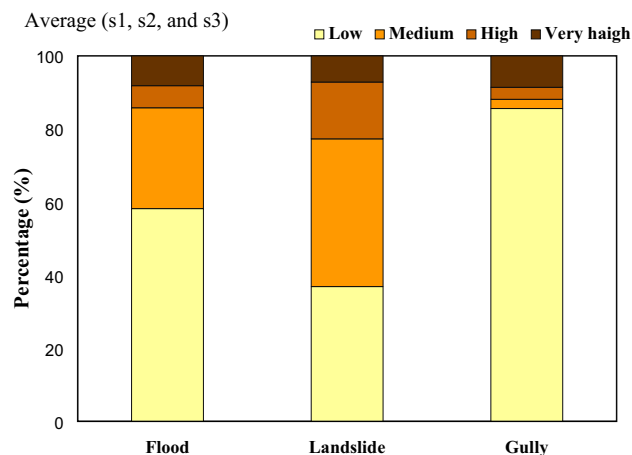


Figure 5. Relative distributions of the average of four susceptibility classes for the flood, landslides, and gully erosion susceptibility maps.

Model	Data set	Probabilistic prediction values	
		Mean	SD
Flood	S1	0.0388	0.1184
	S2	0.0385	0.1151
	S3	0.0383	0.1186
Landslide	S1	0.1422	0.1882
	S2	0.1466	0.1879
	S3	0.1470	0.1884
Gully	S1	0.0437	0.1213
	S2	0.0449	0.1234
	S3	0.0472	0.1284

Table 4. Statistical characteristics of the probability values obtained from ME models. *SD* Standard deviation.

Sensitivity and response curves analysis. A sensitivity analysis^{134,139} was performed to investigate the relative strengths of every predictor variable on the results of predicted maps using the Jackknife test. Suppl. Material 2 shows the results of the Kappa-based Jackknife test using AUC on test data (S1) for flood, landslides, and gully erosion.

Suppl. Material 3 illustrates the response curves of one data set (S1) for some of the important conditioning factors used for three hazards (landslides, flood, and gully erosion) assessment.

The MaxEnt model performance. The results of the MaxEnt model (based on all three sample data sets) show different ranges of susceptibility values of hazards. The results of the goodness-of-fit are shown in Table 5. Figure 6a–c show the AUROC value for the three forecasted hazards maps based on one data set. The hazards samples applied to the model evaluation must be different from the hazards points used for training. In this current work, 30% of hazards occurrence points (30% of floods, landslides, and gully erosion samples) were considered to the validation phase (Table 5). The outcomes of robustness according to AUROC are illustrated in Fig. 7.

Multi-hazard probability map (MHPM). The individual probability maps (i.e., gully erosion, floods, and landslides) which created using the MaxEnt model were used to produce the multi-hazard susceptibility map by synthesizing the three various hazard maps and finally classified into eight different classes: landslides-gully-flood, landslides-floods, landslide-gully, gully erosion, floods, gully-floods, landslides, gully-floods, and no hazard.

Figure 8 shows MHPM of the Gorganrood Watershed for the three hazards. Results demonstrated that 40% of the area is located in the low to very low susceptibility zones whereas 60% of the area is subjected to floods, landslides, and gully occurrence. It is also cleared that the proportion of landslide is the most occupied hazard (21.2%) in the Gorganrood Watershed (i.e. the range of areas covered by a landslide was larger than other hazards) (Fig. 9).

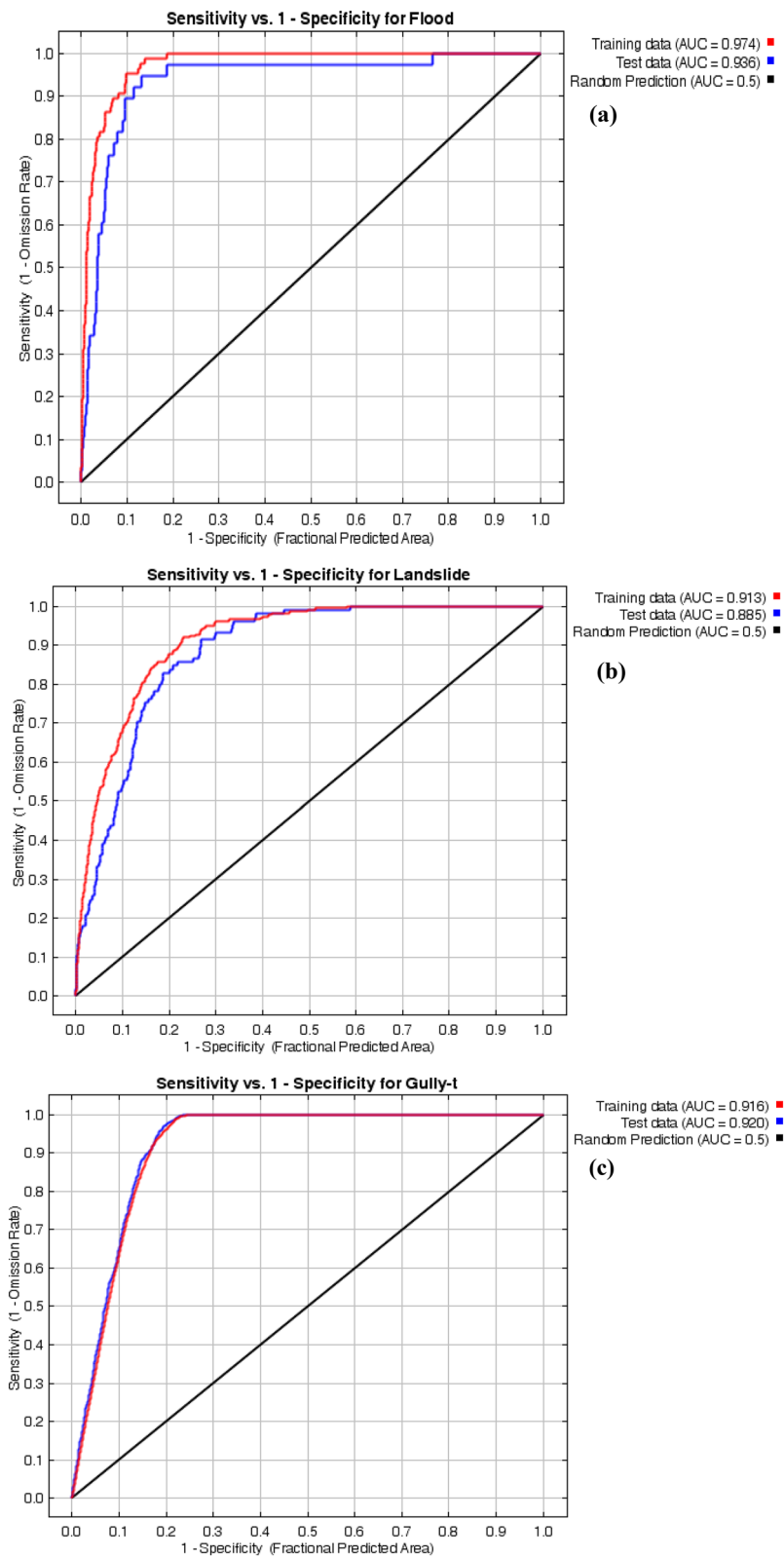


Figure 6. ROC curves of one data set (S1) for three hazards (a) landslides, (b) floods, and (c) gullies.

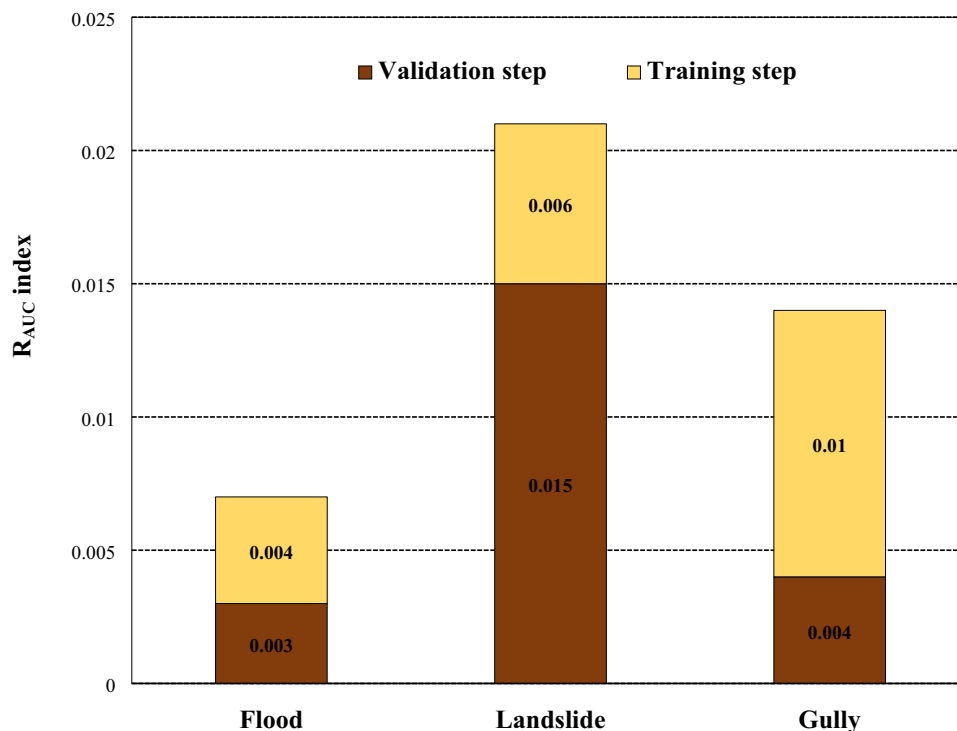


Figure 7. Robustness of the MaxEnt model in training and validation steps based on AUC.

Evaluation criteria (AUC)	Data set	ME model		
		Flood	Landslide	Gully
Training	S1	0.974	0.913	0.916
	S2	0.974	0.914	0.920
	S3	0.970	0.919	0.926
	Mean	0.972	0.915	0.920
Validation	S1	0.936	0.885	0.920
	S2	0.933	0.883	0.918
	S3	0.936	0.870	0.922
	Mean	0.935	0.879	0.92

Table 5. Predictive performance of models based on three sample data sets (S1, S2, and S3) in the training and validation step.

Discussion

Mapping hazards using combined diverse multi-risks. In our current study, after applying the multi-collinearity test, the susceptibility map for each hazard and each dataset was generated using an independent variable. Four susceptibility groups are performed based on the output susceptibility maps using the most authentic natural breaks classifying method^{47,144}.

As Fig. 6 shows, for flood susceptibility mapping according to the MaxEnt model, less than 6% of the study area has a high and very high susceptibility, whereas, about landslides, approximately 14.8% and 8.1% of the study area was classified as high and very high classes, respectively. For the gully erosion susceptibility map, 8.2% of the pixels in the study area fell into high and very high susceptibility classes. For three hazard modelling, the highest percentage belongs to the low class.

Two techniques of one-by-one predictor-removal (OOPR) and only-one-predictor-involved (OOPI) considering the Jackknife-test were used to identify the key hazard-predictors. When isolated, the most influential predictor variables are drainage density, distance to streams, and DEM/elevation, respectively for flood, DEM/elevation, lithological units and annual mean rainfall landslides, and annual mean rainfall, DEM/elevation, lithological units for gully erosion. In other words, the elevation variable was the main controlling factor among all other variables for three hazards, whilst the lithological units were identified as the most important independent variable for gully erosion and landslides.

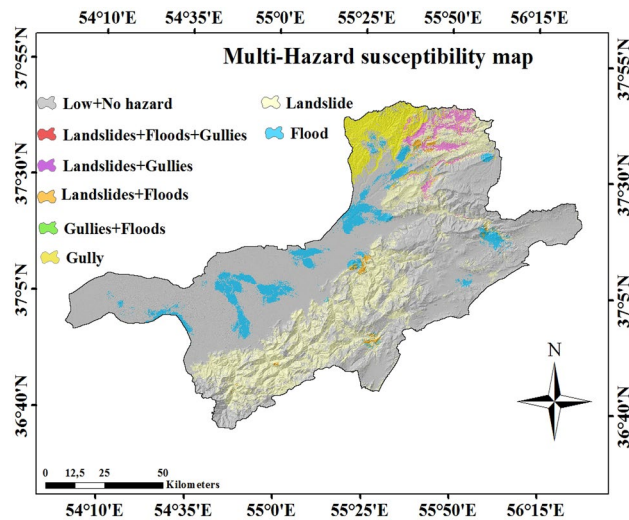


Figure 8. Multi-hazard probability map (MHPM).

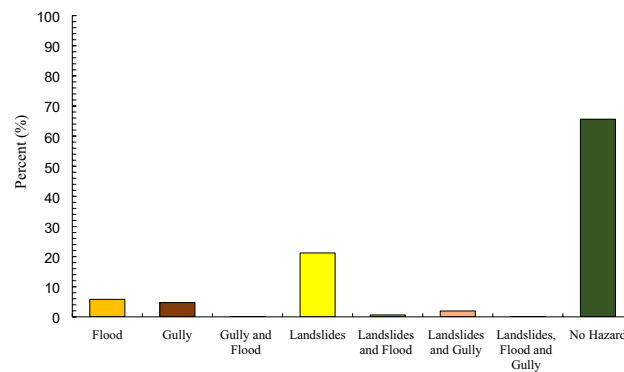


Figure 9. Percent of association of each hazard in the MHPM.

Therefore, as stated by Convertino et al.¹⁴⁵, the SA (sensitivity analysis) allows modelers and managers to identify the conditioning factors (i.e. input variables) that reduce the variance of the model output to the most, which is significantly vital in understanding the model structure.

According to Suppl. Material 3, in the response curve of drainage density, with increasing river density, the flood values increased drastically, the most floods occurred in the range of drainage density between 0.3 and 0.6 km/km². In other words, flood susceptibility increased in the areas with very high drainage density (i.e. increase the runoff transport capacity of drainage network). Based on the outcomes of previous studies, when the drainage density is high, it leads to an important surface runoff ratio. Different factors affect the drainage pattern of an area including slope degree, infiltration rate, vegetation cover condition the structure and nature of the soil characteristics, and geological formation⁸³.

Regarding the distance to streams, the flood happened very close to rivers due to an upsurge in the degree of flood susceptibility. It is one of the important predictor factors owing to its significance on the flood velocity and magnitude. The high concentration of flow in the places around the stream network, there is the most chance of flood incidence close the streams¹¹³. Several studies highlighted that elevation, drainage density, and distance to streams were the most significant predictors for flood occurrence^{103,145,146}.

The flood values decreased in places with high elevation. This was based on the outcomes from response curves of elevation, which demonstrates that flood happens in areas by low elevation and plains. In the areas with low elevation, an abundant amount of water enters the stream network and results in a flood incident¹⁴⁷. The natural treatment of flooding, which happens mostly in flat areas instead of in highly elevated regions can produce a suitable proof for current results. Correspondingly, based on¹⁴⁸, these areas have more upslope contributing area and runoff production. The most landslide occurrences happened in the range of elevation between 300 and 500 m, in which steep slope areas are located. The elevation did not contribute straightly to landslide appearance, but other factors such as precipitation and erosion processes were registered, both of them, logically affected by the elevation, therefore, relevant to be considered too¹⁴⁹. As mentioned by other authors¹⁵⁰, lithological unit structures and attributes constitute fundamental factors in landslide events. Various lithological units based on their types and characteristics have dissimilar landslide possibilities. In response curves of lithological

units to landslide, the most hazard happened in group 21 with Dorud Formation, red sandstone, and shale with subordinate sandy limestone.

The underground hydrostatic level and water pressure surge because of rainfall¹⁵¹. One of the significant operating prognosticators in landslide mapping is landslide initiation which is powerfully connected with rainfall^{151,152}. According to the results, the maximum percentage of the landslide is centralized in areas with rainfall rages from 650 to 690 mm. The gully extension hazard will rise in the high amounts of precipitation¹⁵³. The response curves of rainfall to gully demonstrates the maximum amount of gully erosion that happened in a rainfall ranged from 450 to 500 mm.

Moreover, the elevation has an essential role in the spatial alteration of hydrological conditions for example runoff production rate, soil moisture, surface flow, and slope stability⁶³. Based on the survey of the regions with elevation beneath 200 m and flat areas, our results show that they are more prone to this type of erosion, which can be ascribed to the vegetation cover¹⁵⁴. Consequently, the area with high elevation showed a lower possibility of gully erosion incidence.

Lithological units are considered the most influential prognosticators regarding the gully occurrence¹⁵⁵. The reason was that the parent materials have different hydraulic conductivity and shear stability. In this study, the gully ν within the groups 1 and 13 lithological units with Sanganeh and Sarcheshmeh formations registered this issue, respectively.

Consequently, a relatively higher contribution susceptibility prediction was obtained among some categorical data sets. However, these lesser contributions of some categorical layers did not mean that the categorical data layers were unusable for susceptibility mapping. As discussed in a previous research^{139,156}, all these categorical layers did affect the final prediction result. Then simultaneously considered with continuous data sets.

The results of the goodness-of-fit in Table 5 confirm that performance values for the applied models, based on the AUC-ROC case of flood range from 0.970 to 0.974 (average = 0.972), for landslides, vary from 0.913 to 0.919 (average = 0.915), and for gully erosion, the minimum value of AUC-ROC is 0.916 and the maximum one 0.926 (average = 0.920). Consequently, a high proficiency was acquired for all the three natural hazards studied in this research.

In this current work, 30% of hazards occurrence points were considered to the validation phase (Table 5). Outcomes of the MaxEnt model demonstrates that the AUROC ranges between 0.933–0.936 (average = 0.935) for the floods. In the case of the landslides, AUROC values vary from 0.870 to 0.885 (average = 0.879), whereas for gully erosion changes from 0.918 to 0.922 (average = 0.920). There is a powerful settlement among the output hazard maps of the MaxEnt model and the distribution of hazards occurrence points. According to Hosmer & Lemeshow¹⁴³, the MaxEnt model revealed excellent performances for all datasets^{81,89}. Hence, based on the estimated AUROC value, the employed model detected reasonable prediction proficiency in forecasting the hazard spatial potentiality map. Considering that the accuracy values are almost identical when the data sets change, there were only a few changes and the model for three hazards was robust and entirely stable.

The outcomes of robustness according to AUROC are illustrated in Fig. 7. As can be observed, the MaxEnt model for landslide had a maximum robustness value (0.015) in the validation step indicating the minimum stability and robustness in comparison with other hazards (0.004 and 0.003). Furthermore, from a model stability viewpoint, the almost excellent agreement between training and validation AUC values for the applied model demonstrates that this model is most stable and over-fitting has also been avoided¹⁵⁷. Based on this result, it is obvious that the MaxEnt model can be applied as an efficient machine learning technique in susceptibility assessment for flood, landslides, and gully erosion.

These results are consistent with the study of other authors^{75,157–160}, who intended for preparing susceptibility mapping of the natural disasters.

In this study, we concluded that the MaxEnt is useful to model natural hazards (e.g. flood, landslides, and gully erosion occurrence) with nonlinear relationships. This machine learning model does not need a prior elimination of outliers or data transformation and can fit complex nonlinear relationships between hazards conditioning factors and hazards susceptibility. Also, it is able to automatically analyze interaction effects among conditioning factors (i.e. predictors)⁵⁴. Our results demonstrated that 40% of the area is located in the low to very low susceptibility zones, whereas 60% of the area is subjected to floods, landslides, and gully occurrence. It is also clarified that the relevance of landslides is the most important (21.2%) in the Gorganrood Watershed (Fig. 9).

The most vulnerable areas for human activities are the ones that are in a group of more than one hazard. The flat area with low elevation are more prone to gully erosion and flood in the Gorganrood watershed whilst higher elevation areas with a high slope degree are more susceptible to landslides.

In a similar study, Pourghasemi et al.¹⁶⁰ employed the SWARA-ANFIS-GWO model for producing a multi-hazard susceptibility mapping in Lorestan Province, most sections were susceptible to landslide and flood incidents together (33.7%), although 17.1% of the study region was in the class of no hazards. Nevertheless, in other researches, the various models have been employed for preparing multi-hazard susceptibility mapping. The surveyed hazards were floods, earthquakes, and landslides¹⁶⁰, landslide, earthquake, and floods¹⁶¹, landslides, flood, and forest fire¹⁶², landslides, floods, earthquakes, forest fires, subsidence, and drought¹⁶³, although there were several studies underway to develop multi-hazard risk^{28,35–37}.

Conclusions and final remarks

Using the MaxEnt machine learning technique in the Gorganrood Watershed, we generated individual flood, landslides, and gully erosion susceptibility maps and, subsequently, a combination of them, to estimate a multi-hazard probability map (MHPM). Results showed almost 40% of the area is placed in the low to very low susceptibility zones, but 60% of the area is subjected to floods, landslides, and gully occurrences. The proportion of landslide is the most common hazard in the Gorganrood Watershed (21.2%). Hazard and risk strategies should

be considered before future occurrences. So, this research demonstrates the application of the MHPM may be utilized in other territories for land use planning and hazard mitigation giving new facilities for insurance purposes. To date, there are still no libraries of multi-hazard probability map available for three hazards used in the current study (i.e. flood, landslides, and gully erosion). A conformity procedure is needed to elaborate and design the mitigation practices, provided that individual accomplishments are harmonized with existing policies. Applying a great number of individual hazards maps with spatial covering and various resolutions for the planner is confusing. Therefore, an integrated multi-hazard probability map prepares homogenized data about frequent natural hazards for an area.

Risk and hazard management should be taken into account before studying disaster management. To begin such activities and schematization for further land use planning, the provided flood, gully erosion, and landslide susceptibility maps and the hazard-based probability mapping can be valuable platforms. Multi-hazard evaluation makes it possible reducing hazard risk and gives fundamental information for stakeholders, it can also provide a comprehensive vision of the changes happening in the environment. According to this point, a multi-hazard probability map can be applied for comprehensive and integrated land use planning and consequently for the watershed management.

Received: 11 December 2020; Accepted: 2 March 2021

Published online: 22 March 2021

References

- Mahendra, R., Mohanty, P., Bisoyi, H., Kumar, T. S. & Nayak, S. Assessment and management of coastal multi-hazard vulnerability along the Cuddalore-Villupuram, east coast of India using geospatial techniques. *Ocean Coast. Manag.* **54**, 302–311 (2011).
- Cerdà, A. Effect of climate on surface flow along a climatological gradient in Israel: a field rainfall simulation approach. *J. Arid Environ.* **38**, 145–159 (1998).
- Bathrellos, G. D., Skilodimou, H. D. & Maroukian, H. The spatial distribution of Middle and Late Pleistocene cirques in Greece. *Geogr. Ann. Ser. A Phys. Geogr.* **96**, 323–338 (2014).
- Skilodimou, H. D., Bathrellos, G. D., Maroukian, H. & Gaki-Papanastassiou, K. Late Quaternary evolution of the lower reaches of Ziliana stream in south Mt. Olympus (Greece). *Geogr. Fisica Din. Quatern.* **37**, 43–50 (2014).
- Rodrigo-Comino, J. *et al.* Soil science challenges in a new era: a transdisciplinary overview of relevant topics. *Air Soil Water Res.* **13**, 1178622120977491 (2020).
- García-Ruiz, J. M. Why Geomorphology is a Global Science (2015).
- Ochoa-Cueva, P., Fries, A., Montesinos, P., Rodríguez-Díaz, J. A. & Boll, J. Spatial estimation of soil erosion risk by land-cover change in the Andes of southern Ecuador. *Land Degrad. Dev.* **26**, 565–573 (2015).
- Serrano-Muela, M. P. *et al.* An exceptional rainfall event in the central western Pyrenees: spatial patterns in discharge and impact. *Land Degrad. Dev.* **26**, 249–262 (2015).
- Torres, L., Abraham, E. M., Rubio, C., Barbero-Sierra, C. & Ruiz-Pérez, M. Desertification research in Argentina. *Land Degrad. Dev.* **26**, 433–440 (2015).
- Cerdà, A. Soil water erosion on road embankments in eastern Spain. *Sci. Total Environ.* **378**, 151–155. <https://doi.org/10.1016/j.scitotenv.2007.01.041> (2007).
- Rodrigo-Comino, J., Terol, E., Mora, G., Gimenez-Morera, A. & Cerdà, A. Vicia sativa Roth can reduce soil and water losses in recently planted vineyards (*Vitis vinifera* L.). *Earth Syst. Environ.* **1**, 2. <https://doi.org/10.1007/s41748-020-00191-5> (2020).
- Vorlaufer, T., Falk, T., Dufhues, T. & Kirk, M. Payments for ecosystem services and agricultural intensification: Evidence from a choice experiment on deforestation in Zambia. *Ecol. Econ.* **141**, 95–105. <https://doi.org/10.1016/j.ecolecon.2017.05.024> (2017).
- Kavian, A., Hoseinpoor Sabet, S., Solaimani, K. & Jafari, B. Simulating the effects of land use changes on soil erosion using RUSLE model. *Geocarto Int.* **32**(1), 97–111 (2017).
- Achour, Y. & Pourghasemi, H. R. How do machine learning techniques help in increasing accuracy of landslide susceptibility maps?. *Geosci. Front.* **11**, 871–883. <https://doi.org/10.1016/j.gsf.2019.10.001> (2020).
- Arnaud, P., Bouvier, C., Cisneros, L. & Dominguez, R. Influence of rainfall spatial variability on flood prediction. *J. Hydrol.* **260**, 216–230 (2002).
- Castillo, C. & Gómez, J. A. A century of gully erosion research: urgency, complexity and study approaches. *Earth Sci. Rev.* **160**, 300–319. <https://doi.org/10.1016/j.earscirev.2016.07.009> (2016).
- Kelarestaghi, A. & Ahmadi, H. Landslide susceptibility analysis with a bivariate approach and GIS in Northern Iran. *Arab. J. Geosci.* **2**(1), 95–101 (2009).
- Braud, I. *et al.* Flash floods, hydro-geomorphic response and risk management. *J. Hydrol. Flash Floods Hydro-Geomorphic Response Risk Manag.* **541**, 1–5. <https://doi.org/10.1016/j.jhydrol.2016.08.005> (2016).
- Korup, O., Densmore, A. L. & Schlunegger, F. The role of landslides in mountain range evolution. *Geomorphology* **120**, 77–90. <https://doi.org/10.1016/j.geomorph.2009.09.017> (2010).
- Martínez-Casasnovas, J. A., Ramos, M. C. & García-Hernández, D. Effects of land-use changes in vegetation cover and sidewall erosion in a gully head of the Penedès region (northeast Spain). *Earth Surf. Proc. Land.* **34**, 1927–1937. <https://doi.org/10.1002/esp.1870> (2009).
- Kavian, A. *et al.* Assessing the hydrological effects of land-use changes on a catchment using the Markov chain and WetSpa models. *Hydrol. Sci. J.* **65**(15), 2604–2615 (2020).
- Cutter, S. L., Mitchell, J. T. & Scott, M. S. Revealing the vulnerability of people and places: a case study of Georgetown County, South Carolina. *Ann. Assoc. Am. Geogr.* **90**, 713–737 (2000).
- Alcántara-Ayala, I. Geomorphology, natural hazards, vulnerability and prevention of natural disasters in developing countries. *Geomorphology* **47**, 107–124 (2002).
- Soulard, C. E., Acevedo, W., Stehman, S. V. & Parker, O. P. Mapping extent and change in surface mines within the United States for 2001 to 2006. *Land Degrad. Dev.* **27**, 248–257 (2016).
- Martínez-Graña, A. M., Goy, J. L. & Zazo, C. Cartographic procedure for the analysis of aeolian erosion hazard in natural parks (Central System, Spain). *Land Degrad. Dev.* **26**, 110–117 (2015).
- Strohmeier, S., Laaha, G., Holzmann, H. & Klik, A. Magnitude and occurrence probability of soil loss: a risk analytical approach for the plot scale for two sites in lower Austria. *Land Degrad. Dev.* **27**, 43–51 (2016).
- Weinzierl, T., Wehberg, J., Böhner, J. & Conrad, O. Spatial assessment of land degradation risk for the Okavango River Catchment Southern Africa. *Land Degrad. Dev.* **27**, 281–294 (2016).
- Guzzetti, F., Carrara, A., Cardinali, M. & Reichenbach, P. Landslide hazard evaluation: a review of current techniques and their application in a multi-scale study Central Italy. *Geomorphology* **31**, 181–216 (1999).

29. Friedel, M. J. Modeling hydrologic and geomorphic hazards across post-fire landscapes using a self-organizing map approach. *Environ. Model. Softw.* **26**, 1660–1674 (2011).
30. Mazzorana, B., Comiti, F. & Fuchs, S. A structured approach to enhance flood hazard assessment in mountain streams. *Nat. Hazards* **67**, 991–1009 (2013).
31. Javidan, N., Kaviani, A., Pourghasemi, H. R., Conoscenti, C. H. & Jafarian, Z. Gully erosion susceptibility mapping using multi-variate adaptive regression splines replications and sample size scenarios. *Water* **11**, 1–21. <https://doi.org/10.3390/w1112319> (2019).
32. Agency, F. E. M. Multi-Hazard Identification and Risk Assessment. US Gov. Print (1997).
33. Fema, H.-M. Mr3 Technical Manual. Multi-Hazard Loss Estimation Methodology Earthquake Model (2003).
34. UNISDR, C. The Human Cost of Natural Disasters: A Global Perspective. (2015).
35. Bathrellos, G. D., Kalivas, D. & Skilodimou, H. D. GIS-based landslide susceptibility mapping models applied to natural and urban planning in Trikala Central Greece. *Estud. Geol.* **65**, 49–65 (2009).
36. Das, H., Sonmez, H., Gokceoglu, C. & Nefeslioglu, H. Influence of seismic acceleration on landslide susceptibility maps: a case study from NE Turkey (the Kelkit Valley). *Landslides* **10**, 433–454 (2013).
37. Youssef, A. M. Landslide susceptibility delineation in the Ar-Rayth area, Jizan, Kingdom of Saudi Arabia, using analytical hierarchy process, frequency ratio, and logistic regression models. *Environ. Earth Sci.* **73**, 8499–8518 (2015).
38. Chousianitis, K. *et al.* Assessment of earthquake-induced landslide hazard in Greece: from arias intensity to spatial distribution of slope resistance demand assessment of earthquake-induced landslide hazard in Greece. *Bull. Seismol. Soc. Am.* **106**, 174–188 (2016).
39. Bender, S. Primer on natural hazard management in integrated regional development planning. Organization of American States, Department of Regional Development and Environment. Executive Secretariat for Economic and Social Affairs, Washington, DC (1991).
40. USAID. Primer on Natural Hazard Management in Integrated Regional Development Planning. Department of Regional Development and Environment Executive Secretariat for Economic and Social Affairs Organization of American States. With Support from the Office of Foreign Disaster Assistance United States Agency for International Development Washington, D.C. (Chapter 6) (1991).
41. Kappes, M. S., Keiler, M., von Elverfeldt, K. & Glade, T. Challenges of analyzing multi-hazard risk: a review. *Nat. Hazards* **64**, 1925–1958 (2012).
42. El Morjani, Z. E. A., Ebener, S., Boos, J., Ghaffar, E. A. & Musani, A. Modelling the spatial distribution of five natural hazards in the context of the WHO/EMRO Atlas of Disaster Risk as a step towards the reduction of the health impact related to disasters. *Int. J. Health Geogr.* **6**, 8 (2007).
43. FEMA (Federal Emergency Management Agency). Using HAZUS-MH for risk assessment. HAZU-MH risk assessment and user group series. FEMA 433 (2004).
44. Schmidt, J. *et al.* Quantitative multi-risk analysis for natural hazards: a framework for multi-risk modelling. *Nat. Hazards* **58**, 1169–1192 (2011).
45. Sheikh, V., Kornejady, A. & Ownegh, M. Application of the coupled TOPSIS–Mahalanobis distance for multi-hazard-based management of the target districts of the Golestan Province Iran. *Nat. Hazards* **96**, 1335–1365 (2019).
46. Assimakopoulos, J., Kalivas, D. & Kollias, V. A GIS-based fuzzy classification for mapping the agricultural soils for N-fertilizers use. *Sci. Total Environ.* **309**, 19–33 (2003).
47. Ayalew, L., Yamagishi, H. & Ugawa, N. Landslide susceptibility mapping using GIS-based weighted linear combination, the case in Tsugawa area of Agano River, Niigata Prefecture Japan. *Landslides* **1**, 73–81 (2004).
48. Ayalew, L. & Yamagishi, H. The application of GIS-based logistic regression for landslide susceptibility mapping in the Kakuda-Yahiko Mountains Central Japan. *Geomorphology* **65**, 15–31 (2005).
49. Fernández, D. & Lutz, M. Urban flood hazard zoning in Tucumán Province, Argentina, using GIS and multicriteria decision analysis. *Eng. Geol.* **111**, 90–98 (2010).
50. Peng, S.-H., Shieh, M.-J. & Fan, S.-Y. Potential hazard map for disaster prevention using GIS-based linear combination approach and analytic hierarchy method. *J. Geogr. Inf. Syst.* **4**, 403 (2012).
51. Karaman, H. & Erden, T. Net earthquake hazard and elements at risk (NEAr) map creation for city of Istanbul via spatial multicriteria decision analysis. *Nat. Hazards* **73**, 685–709 (2014).
52. Althuwaynee, O. F., Pradhan, B., Park, H.-J. & Lee, J. H. A novel ensemble bivariate statistical evidential belief function with knowledge-based analytical hierarchy process and multivariate statistical logistic regression for landslide susceptibility mapping. *CATENA* **114**, 21–36 (2014).
53. Karaman, H. *Integrated multi-hazard map creation by using AHP and GIS*. Geomatics Engineering Department, Istanbul Technical University, Recent Advances on Environmental and Life Science (2015).
54. Kornejady, A., Ownegh, M. & Bahremand, A. Landslide susceptibility assessment using maximum entropy model with two different data sampling methods. *CATENA* **152**, 144–162 (2017).
55. Kornejady, A., Ownegh, M., Rahmati, O. & Bahremand, A. Landslide susceptibility assessment using three bivariate models considering the new topo-hydrological factor: HAND. *Geocarto Int.* **33**, 1155–1185 (2018).
56. Chen, W. *et al.* Spatial prediction of landslide susceptibility using an adaptive neuro-fuzzy inference system combined with frequency ratio, generalized additive model, and support vector machine techniques. *Geomorphology* **297**, 69–85 (2017).
57. Devkota, K. C. *et al.* Landslide susceptibility mapping using certainty factor, index of entropy and logistic regression models in GIS and their comparison at Mugling-Narayanghat road section in Nepal Himalaya. *Nat. Hazards* **65**, 135–165 (2013).
58. Pourghasemi, H. R., Jirandeh, A. G., Pradhan, B., Xu, C. & Gokceoglu, C. Landslide susceptibility mapping using support vector machine and GIS at the Golestan Province Iran. *J. Earth Syst. Sci.* **122**, 349–369 (2013).
59. Pourghasemi, H., Moradi, H., Aghda, S. F., Gokceoglu, C. & Pradhan, B. GIS-based landslide susceptibility mapping with probabilistic likelihood ratio and spatial multi-criteria evaluation models (North of Tehran, Iran). *Arab. J. Geosci.* **7**, 1857–1878 (2014).
60. Chen, W. *et al.* A novel hybrid artificial intelligence approach based on the rotation forest ensemble and naïve Bayes tree classifiers for a landslide susceptibility assessment in Langao County, China. *Geomat. Nat. Hazards Risk* **8**, 1955–1977 (2017).
61. Chen, W. *et al.* A novel ensemble approach of bivariate statistical-based logistic model tree classifier for landslide susceptibility assessment. *Geocarto Int.* **33**, 1398–1420 (2018).
62. Chen, W. *et al.* GIS-based landslide susceptibility evaluation using a novel hybrid integration approach of bivariate statistical based random forest method. *CATENA* **164**, 135–149 (2018).
63. Shirzadi, A. *et al.* Novel GIS based machine learning algorithms for shallow landslide susceptibility mapping. *Sensors* **18**(11), 1–28. <https://doi.org/10.3390/s18113777> (2018).
64. Conforti, M., Aucelli, P. P., Robustelli, G. & Scarciglia, F. Geomorphology and GIS analysis for mapping gully erosion susceptibility in the Turbolo stream catchment (Northern Calabria, Italy). *Nat. Hazards* **56**, 881–898 (2011).
65. Park, S., Choi, C., Kim, B. & Kim, J. Landslide susceptibility mapping using frequency ratio, analytic hierarchy process, logistic regression, and artificial neural network methods at the Inje area Korea. *Environ. Earth Sci.* **68**, 1443–1464 (2013).
66. Tehrani, M. S., Lee, M.-J., Pradhan, B., Jebur, M. N. & Lee, S. Flood susceptibility mapping using integrated bivariate and multivariate statistical models. *Environ. Earth Sci.* **72**, 4001–4015 (2014).

67. Mousavi, S. Z., Kaviani, A., Solaimani, K., Mousavi, S. R. & Shirzadi, A. GIS based spatial prediction of landslide susceptibility using logistic regression model. *Geomat. Nat. Hazards Risk* **2**(1), 33–50 (2011).
68. Naghibi, S. A., Pourghasemi, H. R., Pourtaghi, Z. S. & Rezaei, A. Groundwater qanat potential mapping using frequency ratio and Shannon's entropy models in the Moghan watershed Iran. *Earth Sci. Inform.* **8**, 171–186 (2015).
69. Pourghasemi, H. R., Pradhan, B. & Gokceoglu, C. Application of fuzzy logic and analytical hierarchy process (AHP) to landslide susceptibility mapping at Haraz watershed Iran. *Nat. Hazards* **63**, 965–996 (2012).
70. Gómez Gutiérrez, A., Conoscenti, C., Angileri, S., Rotigliano, E. & Schnabel, S. Using topographical attributes to model the spatial distribution of gully erosion from two Mediterranean basins: advantages and limitations. *Nat. Hazards* **10**, 291–314 (2015).
71. Lee, S. Soil erosion assessment and its verification using the universal soil loss equation and geographic information system: a case study at Boun Korea. *Environ. Geol.* **45**, 457–465 (2004).
72. Catani, M., Dell'Acqua, F. & De Schotten, M. T. A revised limbic system model for memory, emotion and behaviour. *Neurosci. Biobehav. Rev.* **37**, 1724–1737 (2013).
73. Conoscenti, C. *et al.* Assessment of susceptibility to earth-flow landslide using logistic regression and multivariate adaptive regression splines: a case of the Belice River basin (western Sicily, Italy). *Geomorphology* **242**, 49–64 (2015).
74. Siahkamari, S., Haghizadeh, A., Zeinivand, H., Tahmasebipour, N. & Rahmati, O. Spatial prediction of flood-susceptible areas using frequency ratio and maximum entropy models. *Geocarto Int.* **33**, 927–941 (2018).
75. Zakerinejad, R. & Märker, M. Prediction of Gully erosion susceptibilities using detailed terrain analysis and maximum entropy modeling: a case study in the Mazayejan Plain, Southwest Iran. *Geogr. Fisica Din. Quaternaria* **37**, 67–76 (2014).
76. Douaik, A., Van Meirvenne, M. & Tóth, T. Soil salinity mapping using spatio-temporal kriging and Bayesian maximum entropy with interval soft data. *Geoderma* **128**, 234–248 (2005).
77. Saghafian, B., Farazjoo, H., Bozorgy, B. & Yazdandoost, F. Flood intensification due to changes in land use. *Water Resour. Manag.* **22**, 1051–1067 (2008).
78. [CONRWMGP] Central Office of Natural Resources and Watershed Management in Golestan Province. Detailed action plan. Iran; p. 230 (2009).
79. Sharifi, F. & Mahdavi, M. Technical report on investigating causes of summer flooding on North-east of Golestan-Iran deputy of watershed management-Iran. *Iran. J. Watershed Manag.* **60**, 85–110 (2001).
80. Water Resources Company of Golestan [WRCG]. Precipitation and temperature reports; [cited 2013 August 11]. <http://www.gsrw.ir/Default.aspx> (2013).
81. Conoscenti, C. *et al.* Gully erosion susceptibility assessment by means of GIS-based logistic regression: a case of Sicily (Italy). *Geomorphology* **204**, 399–411 (2014).
82. Manandhar, B. *Flood Plain Analysis and Risk Assessment of Lothar Khola*. Master of Science Thesis in Watershed Management. Tribhuvan University Institute of Forestry Pokhara, Nepal (2010).
83. Pourtaghi, Z. S. & Pourghasemi, H. R. GIS-based groundwater spring potential assessment and mapping in the Birjand Township, southern Khorasan Province Iran. *Hydrogeol. J.* **22**, 643–662 (2014).
84. Rahmati, O., Pourghasemi, H. R. & Melesse, A. M. Application of GIS-based data driven random forest and maximum entropy models for groundwater potential mapping: a case study at Mehran Region Iran. *CATENA* **137**, 360–372 (2016).
85. Angileri, S. E. *et al.* Water erosion susceptibility mapping by applying stochastic gradient treeboost to the Imera Meridionale river basin (Sicily, Italy). *Geomorphology* **262**, 61–76 (2016).
86. Cama, M., Lombardo, L., Conoscenti, C. & Rotigliano, E. Improving transferability strategies for debris flow susceptibility assessment: application to the Saponara and Itala catchments (Messina, Italy). *Geomorphology* **288**, 52–65 (2017).
87. Kia, M. B. *et al.* An artificial neural network model for flood simulation using GIS: Johor River Basin Malaysia. *Environ. Earth Sci.* **67**, 251–264 (2012).
88. Tehrani, M. S., Pradhan, B. & Jebur, M. N. Flood susceptibility mapping using a novel ensemble weights-of-evidence and support vector machine models in GIS. *J. Hydrol.* **512**, 332–343 (2014).
89. Conoscenti, C. *et al.* Exploring the effect of absence selection on landslide susceptibility models: a case study in Sicily Italy. *Geomorphology* **261**, 222–235 (2016).
90. Jiménez-Perálvarez, J., Irigaray, C., El Hamdouni, R. & Chacón, J. Landslide-susceptibility mapping in a semi-arid mountain environment: an example from the southern slopes of Sierra Nevada (Granada, Spain). *Bull. Eng. Geol. Environ.* **70**, 265–277 (2011).
91. Saponaro, A. *et al.* Landslide susceptibility analysis in data-scarce regions: the case of Kyrgyzstan. *Bull. Eng. Geol. Environ.* **74**, 1117–1136 (2015).
92. Jaafari, A., Najafi, A., Pourghasemi, H., Rezaeian, J. & Sattarian, A. GIS-based frequency ratio and index of entropy models for landslide susceptibility assessment in the Caspian forest, northern Iran. *Int. J. Environ. Sci. Technol.* **11**, 909–926 (2014).
93. Nagarajan, R., Roy, A., Kumar, R. V., Mukherjee, A. & Khire, M. Landslide hazard susceptibility mapping based on terrain and climatic factors for tropical monsoon regions. *Bull. Eng. Geol. Environ.* **58**, 275–287 (2000).
94. Gallardo-Cruz, J. A., Pérez-García, E. A. & Meave, J. A. β -Diversity and vegetation structure as influenced by slope aspect and altitude in a seasonally dry tropical landscape. *Landscape Ecol.* **24**, 473–482 (2009).
95. Geroy, I. *et al.* Aspect influences on soil water retention and storage. *Hydrol. Process.* **25**, 3836–3842 (2011).
96. Lucà, F., Conforti, M. & Robustelli, G. Comparison of GIS-based gully erosion susceptibility mapping using bivariate and multivariate statistics: Northern Calabria South Italy. *Geomorphology* **134**, 297–308 (2011).
97. Ercanoglu, M. & Gokceoglu, C. Assessment of landslide susceptibility for a landslide-prone area (north of Yenice, NW Turkey) by fuzzy approach. *Environ. Geol.* **41**, 720–730 (2002).
98. Sidle, R. & Ochiai, H. Processes, Prediction, and Land Use. *Water Resources Monograph. American Geophysical Union, Washington* (2006).
99. Yalcin, A. GIS-based landslide susceptibility mapping using analytical hierarchy process and bivariate statistics in Ardesen (Turkey): comparisons of results and confirmations. *CATENA* **72**, 1–12 (2008).
100. Vahidnia, M. H., Alesheikh, A. A., Alimohammadi, A. & Hosseinali, F. A GIS-based neuro-fuzzy procedure for integrating knowledge and data in landslide susceptibility mapping. *Comput. Geosci.* **36**, 1101–1114 (2010).
101. Poiraud, A. Landslide susceptibility–certainty mapping by a multi-method approach: a case study in the Tertiary basin of Puy-en-Velay (Massif central, France). *Geomorphology* **216**, 208–224 (2014).
102. Meinhardt, M., Fink, M. & Tüschel, H. Landslide susceptibility analysis in central Vietnam based on an incomplete landslide inventory: comparison of a new method to calculate weighting factors by means of bivariate statistics. *Geomorphology* **234**, 80–97 (2015).
103. Khosravi, K., Nohani, E., Maroufinia, E. & Pourghasemi, H. R. A GIS-based flood susceptibility assessment and its mapping in Iran: a comparison between frequency ratio and weights-of-evidence bivariate statistical models with multi-criteria decision-making technique. *Nat. Hazards* **83**, 947–987 (2016).
104. Moghaddam, D. D., Rezaei, M., Pourghasemi, H., Pourtaghi, Z. & Pradhan, B. Groundwater spring potential mapping using bivariate statistical model and GIS in the Taleghan watershed Iran. *Arab. J. Geosci.* **8**, 913–929 (2015).
105. Jenness, J. DEM surface tools for ArcGIS (2013).
106. Maestre, F. T. & Cortina, J. Spatial patterns of surface soil properties and vegetation in a Mediterranean semi-arid steppe. *Plant Soil* **241**, 279–291 (2002).

107. Cosby, B., Hornberger, G., Clapp, R. & Ginn, T. A statistical exploration of the relationships of soil moisture characteristics to the physical properties of soils. *Water Resour. Res.* **20**, 682–690 (1984).
108. Gyssels, G., Poesen, J., Nachtergaele, J. & Govers, G. The impact of sowing density of small grains on rill and ephemeral gully erosion in concentrated flow zones. *Soil Tillage Res.* **64**, 189–201 (2002).
109. Vandekerckhove, L., Poesen, J. & Govers, G. Medium-term gully headcut retreat rates in Southeast Spain determined from aerial photographs and ground measurements. *CATENA* **50**, 329–352 (2003).
110. De Reu, J. *et al.* Application of the topographic position index to heterogeneous landscapes. *Geomorphology* **186**, 39–49 (2013).
111. Moore, I. D. & Grayson, R. B. Terrain-based catchment partitioning and runoff prediction using vector elevation data. *Water Resour. Res.* **27**, 1177–1191 (1991).
112. Grabs, T., Seibert, J., Bishop, K. & Laudon, H. Modeling spatial patterns of saturated areas: a comparison of the topographic wetness index and a dynamic distributed model. *J. Hydrol.* **373**, 15–23 (2009).
113. Glenn, E. P. *et al.* Roles of saltcedar (*Tamarix* spp.) and capillary rise in salinizing a non-flooding terrace on a flow-regulated desert river. *J. Arid Environ.* **79**, 56–65 (2012).
114. Kamp, U., Growley, B. J., Khattak, G. A. & Owen, L. A. GIS-based landslide susceptibility mapping for the 2005 Kashmir earthquake region. *Geomorphology* **101**, 631–642 (2008).
115. Jungerius, P., Matundura, J. & Van De Ancker, J. Road construction and gully erosion in West Pokot Kenya. *Earth Surf. Process. Landf.* **27**, 1237–1247 (2002).
116. Shimizu, M. In *International Symposium on Landslides*. 5. 771–776.
117. Lan, H., Zhou, C., Wang, L., Zhang, H. & Li, R. Landslide hazard spatial analysis and prediction using GIS in the Xiaojiang watershed, Yunnan China. *Eng. Geol.* **76**, 109–128 (2004).
118. Duc, D. M. Rainfall-triggered large landslides on 15 December 2005 in Van Canh district, Binh Dinh province Vietnam. *Landslides* **10**, 219–230 (2013).
119. Bui, D. T., Pradhan, B., Lofman, O., Revhaug, I. & Dick, O. B. Landslide susceptibility mapping at Hoa Binh province (Vietnam) using an adaptive neuro-fuzzy inference system and GIS. *Comput. Geosci.* **45**, 199–211 (2012).
120. Nefeslioglu, H. A., Gokceoglu, C. & Sonmez, H. An assessment on the use of logistic regression and artificial neural networks with different sampling strategies for the preparation of landslide susceptibility maps. *Eng. Geol.* **97**, 171–191 (2008).
121. Kakembo, V., Xanga, W. & Rowntree, K. Topographic thresholds in gully development on the hillslopes of communal areas in Ngqushwa Local Municipality, Eastern Cape South Africa. *Geomorphology* **110**, 188–194 (2009).
122. Böhner, J. & Selige, T. *Spatial Prediction of Soil Attributes Using Terrain Analysis and Climate Regionalisation* (2006).
123. Song, Y. *et al.* Susceptibility assessment of earthquake-induced landslides using Bayesian network: a case study in Beichuan China. *Comput. Geosci.* **42**, 189–199 (2012).
124. Zhu, A.-X. *et al.* An expert knowledge-based approach to landslide susceptibility mapping using GIS and fuzzy logic. *Geomorphology* **214**, 128–138 (2014).
125. Miller, J. R. Morphometric assessment of lithologic controls on drainage basin evolution in the Crawford Upland, South-Central Indiana Jerry R. Miller, Dale F. Ritter, and R. Craig Kochel. *Am. J. Sci.* **290**, 569–599 (1990).
126. Renard, K. G. *Predicting Soil Erosion by Water: A Guide to Conservation Planning with the Revised Universal Soil Loss Equation (RUSLE)*. (United States Government Printing, 1997).
127. Moore, I. D. & Burch, G. J. Physical basis of the length-slope factor in the Universal Soil Loss Equation. *Soil Sci. Soc. Am. J.* **50**, 1294–1298 (1986).
128. Farrar, D. E. & Glauber, R. R. Multicollinearity in regression analysis: the problem revisited. *Rev. Econ. Stat.* **49**, 92–107 (1967).
129. O'Brien, R. M. A caution regarding rules of thumb for variance inflation factors. *Qual. Quant.* **41**, 673–690 (2007).
130. Ozdemir, A. Using a binary logistic regression method and GIS for evaluating and mapping the groundwater spring potential in the Sultan Mountains (Aksehir, Turkey). *J. Hydrol.* **405**, 123–136 (2011).
131. Phillips, S. J., Anderson, R. P. & Schapire, R. E. Maximum entropy modeling of species geographic distributions. *Ecol. Model.* **190**, 231–259 (2006).
132. Phillips, S. J., Dudík, M. & Schapire, R. E. In *Proceedings of the Twenty-First International Conference on Machine Learning*. **83**.
133. Medley, K. A. Niche shifts during the global invasion of the Asian tiger mosquito, *Aedes albopictus* Skuse (Culicidae), revealed by reciprocal distribution models. *Glob. Ecol. Biogeogr.* **19**, 122–133 (2010).
134. Moreno, R., Zamora, R., Molina, J. R., Vasquez, A. & Herrera, M. Á. Predictive modeling of microhabitats for endemic birds in South Chilean temperate forests using Maximum entropy (MaxEnt). *Ecol. Inform.* **6**, 364–370 (2011).
135. Boubli, J. & De Lima, M. Modeling the geographical distribution and fundamental niches of *Cacajao* spp. and *Chiropotes israelita* in Northwestern Amazonia via a maximum entropy algorithm. *Int. J. Primatol.* **30**, 217–228 (2009).
136. Archer, G., Saltelli, A. & Sobol, I. Sensitivity measures, ANOVA-like techniques and the use of bootstrap. *J. Stat. Comput. Simul.* **58**, 99–120 (1997).
137. Chen, Y. *et al.* CaliBayes and BASIS: integrated tools for the calibration, simulation and storage of biological simulation models. *Brief Bioinform.* **11**, 278–289 (2010).
138. Yost, A. C., Petersen, S. L., Gregg, M. & Miller, R. Predictive modeling and mapping sage grouse (*Centrocercus urophasianus*) nesting habitat using maximum entropy and a long-term dataset from Southern Oregon. *Ecol. Inform.* **3**, 375–386 (2008).
139. Park, N.-W. Using maximum entropy modeling for landslide susceptibility mapping with multiple geoenvironmental data sets. *Environ. Earth Sci.* **73**, 937–949 (2015).
140. Chung, C.-J.F. & Fabbri, A. G. Validation of spatial prediction models for landslide hazard mapping. *Nat. Hazards* **30**, 451–472 (2003).
141. Maier, H. R. & Dandy, G. C. Neural networks for the prediction and forecasting of water resources variables: a review of modeling issues and applications. *Environ. Model. Softw.* **15**, 101–124 (2000).
142. Swets, J. A. Measuring the accuracy of diagnostic systems. *Science* **240**, 1285–1293 (1988).
143. Hosmer, D. W. *Wiley Series in Probability and Statistics*, Chap. 2. Multiple Logistic Regression. *Applied Logistic Regression*, 31–46 (2000).
144. Akgun, A., Dag, S. & Bulut, F. Landslide susceptibility mapping for a landslide-prone area (Findikli, NE of Turkey) by likelihood-frequency ratio and weighted linear combination models. *Environ. Geol.* **54**, 1127–1143 (2008).
145. Convertino, M., Muñoz-Carpena, R., Chu-Agor, M. L., Kiker, G. A. & Linkov, I. Untangling drivers of species distributions: global sensitivity and uncertainty analyses of MaxEnt. *Environ. Model. Softw.* **51**, 296–309 (2014).
146. Bui, D. T. *et al.* Hybrid artificial intelligence approach based on neural fuzzy inference model and metaheuristic optimization for flood susceptibility modeling in a high-frequency tropical cyclone area using GIS. *J. Hydrol.* **540**, 317–330 (2016).
147. Lee, S., Kim, J.-C., Jung, H.-S., Lee, M. J. & Lee, S. Spatial prediction of flood susceptibility using random-forest and boosted-tree models in Seoul metropolitan city, Korea. *Geomat. Nat. Hazards Risk* **8**, 1185–1203 (2017).
148. Mojaddadi, H., Pradhan, B., Nampak, H., Ahmad, N. & Ghazali, A. H. B. Ensemble machine-learning-based geospatial approach for flood risk assessment using multi-sensor remote-sensing data and GIS. *Geomat. Nat. Hazards Risk* **8**, 1080–1102 (2017).
149. Rozos, D., Pyrgiotis, L., Skias, S. & Tsagaratos, P. An implementation of rock engineering system for ranking the instability potential of natural slopes in Greek territory. An application in Karditsa County. *Landslides* **5**, 261–270 (2008).
150. Yalcin, A. *An Investigation on Ardesen (Rize) Region on the Basis of Landslide Susceptibility*, Ph. D. Dissertation. Karadeniz Technical University, Trabzon, Turkey (2005).

151. Shahabi, H., Ahmad, B. B. & Khezri, S. Application of satellite remote sensing for detailed landslide inventories using frequency ratio model and GIS. *Int. J. Comput. Sci.* **9**, 108–117 (2012).
152. Shahabi, H., Khezri, S., Ahmad, B. B. & Hashim, M. Landslide susceptibility mapping at central Zab basin, Iran: a comparison between analytical hierarchy process, frequency ratio and logistic regression models. *CATENA* **115**, 55–70 (2014).
153. Svoray, T., Michailov, E., Cohen, A., Rokah, L. & Sturm, A. Predicting gully initiation: comparing data mining techniques, analytical hierarchy processes and the topographic threshold. *Earth Surf. Proc. Land.* **37**, 607–619 (2012).
154. Daba, S., Rieger, W. & Strauss, P. Assessment of gully erosion in eastern Ethiopia using photogrammetric techniques. *CATENA* **50**, 273–291 (2003).
155. Dai, F., Lee, C., Li, J. & Xu, Z. Assessment of landslide susceptibility on the natural terrain of Lantau Island Hong Kong. *Environ. Geol.* **40**, 381–391 (2001).
156. Marmion, M., Hjort, J., Thuiller, W. & Luoto, M. A comparison of predictive methods in modelling the distribution of periglacial landforms in Finnish Lapland. *Earth Surf. Proc. Land.* **33**, 2241–2254 (2008).
157. Golkarian, A. & Rahmati, O. Use of a maximum entropy model to identify the key factors that influence groundwater availability on the Gonabad Plain Iran. *Environ. Earth Sci.* **77**, 369 (2018).
158. Pournader, M., Ahmadi, H., Feiznia, S., Karimi, H. & Peirovan, H. R. Spatial prediction of soil erosion susceptibility: an evaluation of the maximum entropy model. *Earth Sci. Inf.* **11**, 389–401 (2018).
159. Moghaddam, D. D., Pourghasemi, H. R. & Rahmati, O. *Natural Hazards GIS-Based Spatial Modeling Using Data Mining Techniques* 59–78 (Springer, 2019).
160. Pourghasemi, H. R., Gayen, A., Panahi, M., Rezaie, F. & Blaschke, T. Multi-hazard probability assessment and mapping in Iran. *Sci. Total Environ.* **692**, 556–571 (2019).
161. Skilodimou, H. D., Bathrellos, G. D., Chousianitis, K., Youssef, A. M. & Pradhan, B. Multi-hazard assessment modeling via multi-criteria analysis and GIS: a case study. *Environ. Earth Sci.* **78**, 47 (2019).
162. Pourghasemi, H. R., Gayen, A., Edalat, M., Zarafshar, M. & Tiefenbacher, J. P. Is multi-hazard mapping effective in assessing natural hazards and integrated watershed management?. *Geosci. Front.* **11**, 1203–1217 (2020).
163. Pourghasemi, H. R. *et al.* Assessing and mapping multi-hazard risk susceptibility using a machine learning technique. *Sci. Rep.* **10**, 1–11 (2020).

Acknowledgements

The authors would like to thank the Regional Water Authority and Natural Resources and Watershed Management Department of Golestan province for providing the discharge and meteorological data and some initial maps. We would also like to thank Sari Agricultural Sciences and Natural Resources University (SANRU) for funding the project.

Author contributions

N.J., A.K., H.R.P., C.C., Z.J., J.R.C. designed experiments, run models, analyzed results, wrote, and reviewed manuscript. All authors reviewed the final manuscript.

Funding

Open Access funding enabled and organized by Projekt DEAL.

Competing interests

The authors declare no competing interests.

Additional information

Supplementary Information The online version contains supplementary material available at <https://doi.org/10.1038/s41598-021-85862-7>.

Correspondence and requests for materials should be addressed to A.K. or J.R.-C.

Reprints and permissions information is available at www.nature.com/reprints.

Publisher's note Springer Nature remains neutral with regard to jurisdictional claims in published maps and institutional affiliations.



Open Access This article is licensed under a Creative Commons Attribution 4.0 International License, which permits use, sharing, adaptation, distribution and reproduction in any medium or format, as long as you give appropriate credit to the original author(s) and the source, provide a link to the Creative Commons licence, and indicate if changes were made. The images or other third party material in this article are included in the article's Creative Commons licence, unless indicated otherwise in a credit line to the material. If material is not included in the article's Creative Commons licence and your intended use is not permitted by statutory regulation or exceeds the permitted use, you will need to obtain permission directly from the copyright holder. To view a copy of this licence, visit <http://creativecommons.org/licenses/by/4.0/>.

© The Author(s) 2021